THE JOURNAL OF PHYSICAL CHEMISTRY C

Article

pubs.acs.org/JPCC

# Interplay of Confinement and Surface Energetics in the Interaction of Water with a Metal−Organic Framework

Di Wu,[†] Xiaofeng Guo,[†,‡] Hui Sun,[§] and Alexandra Navrotsky*[,†]

[†]Peter A. Rock Thermochemistry Laboratory and NEAT ORU, University of California, Davis, One Shields Avenue, Davis, California 95616, United States

[‡]Earth System Observations, Earth and Environmental Sciences Division, Los Alamos National Laboratory, Los Alamos, New Mexico 87545, United States

[§]State Key Laboratory of Chemical Engineering, East China University of Science and Technology, Shanghai 200237, China

Supporting Information

**ABSTRACT:** The enthalpy of water adsorption ($\Delta h$) on the metal−organic framework (MOF) HKUST-1 has been determined directly by calorimetry. The most exothermic value of $\Delta h$ [−119.4 ± 0.5 kJ/(mol of water)] occurs at zero coverage and perhaps represents water confinement in the smallest (4-Å) cages. An intermediate $\Delta h$ value of −50.2 ± 1.8 kJ/(mol of water) at higher loading probably corresponds to the binding of water on the available Cu nodes and subsequent filling of the largest (11-Å) pores. The weakest interactions take place in the medium (10-Å) cages, showing weak inclusion of water clusters in a limited hydrophobic environment. By combining ethanol adsorption calorimetry, mathematical analysis of the slope of the water adsorption isotherm, and the differential enthalpy of water adsorption curve, we are able not only to develop an approach to separate energetically multistage guest−host interactions in complex MOF architectures but also to distinguish a sequence of interactions with very similar energetic effects.

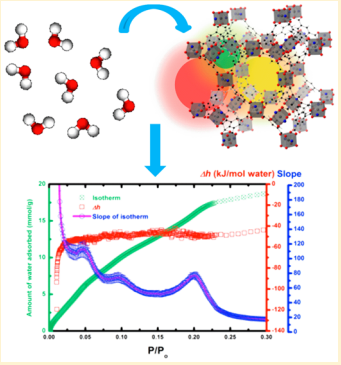


## INTRODUCTION

Metal−organic frameworks (MOFs) are a unique class of crystalline nanoporous hybrid materials that can be synthesized through the assembly of metal ions and organic linkers under solventhermal/hydrothermal conditions.[1−5] Owing to their extremely open nanoporosity, large accessible surface areas, and chemically editable hybrid architectures, MOFs are very promising for applications in heterogeneous catalysis,[6] gas sorption and separation,[7−11] energy storage,[2,12] drug delivery,[13] and molecular/electronic sensing.[14] HKUST-1, one of the most widely investigated MOF structures, is constructed by Cu paddle-wheel secondary building units (SBUs) that are directly coordinated by benzene-1,3,5-tricarboxylic acid (BTC) linkers.[15] The complex three-dimensional structure of HKUST-1 involves three different interconnected pores/cages (4, 10, and 11 Å; see Figure 1A).[15] The small cages (4 Å) are located at the corners of medium and large pores. However, their apertures open only into the 11-Å pores. The medium and large pores are arranged alternately and open into each other. The exposed Cu coordination sites can be accessed only in the 11-Å cages, making the pore surface hydrophilic.[16] Although HKUST-1 has been commercialized by BASF as Basolite C 300,[17−19] the understanding of confinement of small molecules with freshly activated HKUST-1 is still largely empirical. The interaction of MOFs with water is especially important because of their high surface areas, their frequent degradation by moisture, and the pervasive presence of $H_2O$ in laboratory and industrial settings. Hence, it is essential to perform a thorough fundamental investigation of the energetics of water−MOF systems to reveal the underlying interactions and competition among different bonding factors.

Herein, we report a direct gas adsorption calorimetric study using water as a probe molecule to elucidate guest−host interaction details in HKUST-1, which features two distinct types of surfaces (hydrophobic and hydrophilic) and three different sizes of pores/cages.[15] The adsorption calorimetry apparatus (Figure 1B) developed in our laboratory consists of a Calvet-type microcalorimeter coupled with a commercial gas adsorption analyzer to enable precise control of vapor dosing and accurate detection of heat associated with each small dose of gas.[20] Previously, we employed this system mainly to investigate the surface energy of inorganic oxide nanoparticles.[21−24] Recently, we applied this method to study $CO_2$ capture and $CH_4$ storage on various MOFs,[25−27] demonstrating that direct gas adsorption calorimetry has great advantages for evaluating gas−MOF interactions at low pressure, which exhibit strong exothermic heat effects at zero coverage (steep initial isotherms) and multistrength adsorption events (stepwise differential enthalpy curves) at various operating temperatures. In the present study, for the first time, we applied biprobe (water and ethanol) adsorption calorimetry to HKUST-1 along with mathematical analysis of the isotherm to determine the

**Received:** December 14, 2015
**Revised:** March 23, 2016
**Published:** March 24, 2016





DOI: 10.1021/acs.jpcc.5b12239
J. Phys. Chem. C 2016, 120, 7562−7567

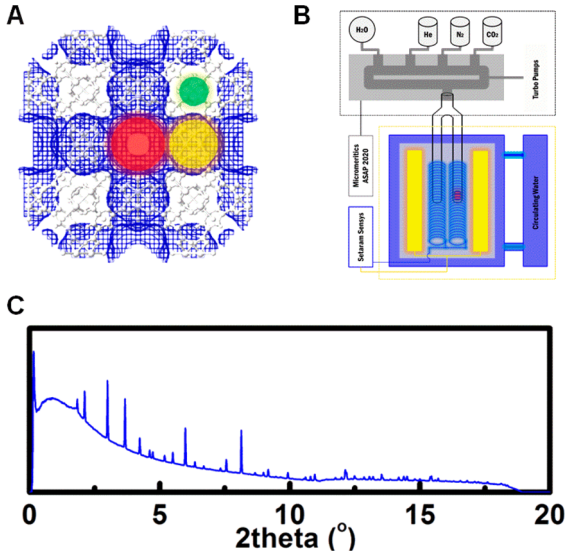


**Figure 1.** (A) Illustration of the HKUST-1 structure in a two-dimensional view along the (100) direction. Spherical shapes represent the small pores (4 Å, green), medium pores (10 Å, yellow), and large pores (11 Å, red). (B) Schematic of the experimental setup for water adsorption calorimetry on HKUST-1. (C) X-ray scattering pattern of activated HKUST-1.

enthalpy of adsorption as a function of water loading from zero coverage to water saturation, to identify different strengths of interactions at various positions (cages and sites), to separate interactions with similar magnitudes, and to interpret the binding mechanisms with an emphasis on the interplay and competition of confinement effects and surface adsorption.

## EXPERIMENTAL METHODS

The source and characterization of the HKUST-1 used in this work (X-ray diffraction patterns, nitrogen adsorption−desorption isotherms, and thermal analysis) were published elsewhere.[28] Synchrotron X-ray scattering was performed at the B1 station of the Cornell High Energy Synchrotron Source (CHESS) using an angle-dispersive geometry. Activated HKUST-1 was placed into a chamber (200 $\mu$m in diameter and 100 $\mu$m in thickness) that was set on the flat surface of a transparent diamond window. The white X-rays were collimated into a monochromatic beam (0.485946 Å) by a double-crystal monochromator. A large MAR345 image plate detector was employed to collect the scattering signals. The obtained two-dimensional image was integrated into one-dimensional patterns as a function of $2\theta$ (degrees) for structural analysis using Fit2D software.

The enthalpies of water sorption were determined directly by gas adsorption calorimetry at 25 °C as described by Ushakov and Navrotsky.[20] The apparatus (Figure 1B) includes a Calvet-type microcalorimeter (Setaram SenSYS) coupled to a commercial adsorption analyzer (Micromeritics ASAP 2020). HKUST-1 crystals (~50 mg) were loaded into one side of a custom-made silica glass forked tube, the other side of which remained empty as a reference. This tube was introduced into the twin chambers of the calorimeter and attached to the gas-adsorption analyzer for degassing and further analyses. Prior to each analysis, the sample was evacuated ($<10^{-3}$ Pa) for 24 h at 180 °C to avoid insufficient activation. The ASAP 2020 instrument was programmed to operate in incremental dosing mode with 1 $\mu$mol per dose and 1.0−1.5 h equilibration periods. The amount of gas adsorbed from each dose was recorded by the gas adsorption analyzer, and the associated heat effect was detected simultaneously by the micro-calorimeter. Processing software (AKTS, Switzerland) was employed to extract enthalpies of adsorption (kilojoules per mole of molecules). Ethanol (pure, anhydrous alcohol, Fluka) adsorption calorimetry (1 $\mu$mol per dose and 1.0−1.5 h equilibration periods) was also designed and performed using the same instrument to assist the interpretation of the water−HKUST-1 interactions.

## RESULTS

The synchrotron X-ray scattering pattern of activated HKUST-1 is presented in Figure 1C, which confirms its structure and phase purity.[15] The adsorption isotherm and associated

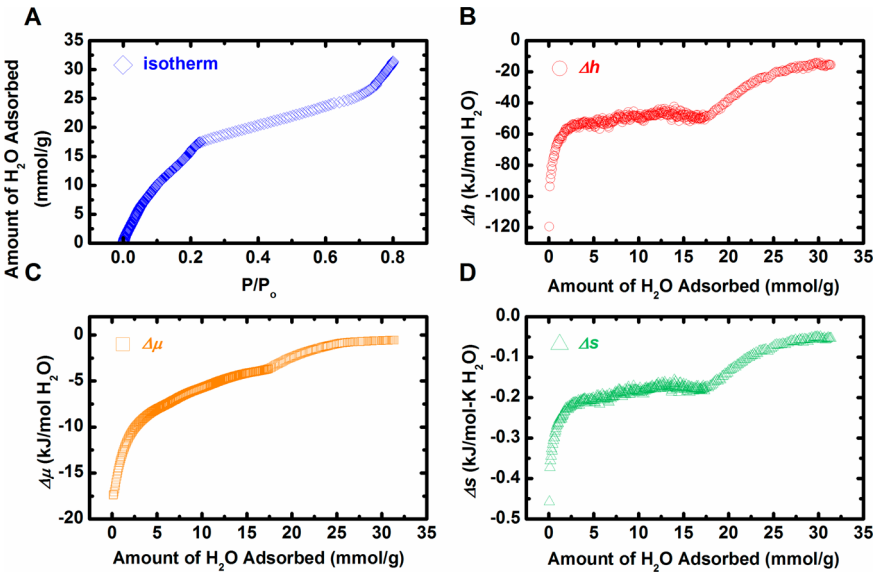


**Figure 2.** (A) Water adsorption isotherm, (B) differential enthalpy of adsorption curve, (C) partial molar free energy (chemical potential) of adsorption curve, and (D) differential entropy of adsorption curve for water adsorption on HKUST-1 at 25 °C.



DOI: 10.1021/acs.jpcc.5b12239
J. Phys. Chem. C 2016, 120, 7562−7567

differential enthalpy of adsorption ($\Delta h$) curve are presented in panels A and B, respectively, of Figure 2. The $\Delta h$ values are also listed in Table 1. For water adsorption on freshly activated HKUST-1, the most exothermic differential enthalpy of adsorption is $-119.4 \pm 0.5$ kJ/(mol of water). This finding complements simulation results[29,30] and solution calorimetric data[28] by providing enthalpies at zero coverage, which cannot be accurately measured by other methods. As the water loading is increased, the differential enthalpy of adsorption changes sharply to a less exothermic plateau of $-50.2 \pm 1.8$ kJ/(mol of water) between 2.7 and 17.8 mmol/g. This is an indication of chemisorption into a site or set of sites of constant or almost constant average energy. Beyond 17.8 mmol/g, the enthalpy of adsorption becomes less exothermic, gradually ramping up to the second plateau at $-15.2 \pm 2.3$ kJ/(mol of water) at 29.9 mmol/g. This weak physisorption, which has not been described in previous investigations, is much less exothermic than that of water condensation [−44.0 kJ/(mol of water)]. The degree of hydrophobicity is comparable to what was observed for the dehydroxylated silica surface.[23]

**Table 1. Differential Enthalpy of Water Adsorption on HKUST-1 as a Function of the Amount of Water Adsorbed**

| amount of water adsorbed [mmol/(g of HKUST-1)] | differential enthalpy of water adsorption [kJ/(mol of water)] |
|---|---|
| ~0.0 | $-119.4 \pm 0.5$ |
| 2.7−17.8 | $-50.2 \pm 1.8$ |
| >29.9 | $-15.2 \pm 2.3$ |

The partial molar free energy (chemical potential, $\Delta\mu$) of water adsorption directly derived from the isotherm is presented in Figure 2C. It becomes less exothermic as the reaction proceeds. Combining the differential enthalpy of adsorption with the partial molar free energy, one obtains the partial molar entropy ($\Delta s$) of water adsorption using the relation $\Delta\mu = \Delta h - T\Delta s$ (Figure 2D). $\Delta s$ becomes less negative as more water is adsorbed. Hence, all partial molar properties indicate a fading overall driving force for the reaction as the water coverage or partial pressure increases. Although a diminishing strength of adsorption with increasing coverage is typical, the two plateaus suggest complexity not generally seen in inorganic frameworks.

## DISCUSSION

HKUST-1 has three types of cages, one relatively hydrophilic (11 Å) with Cu coordinating sites and two smaller pores (4 and 10 Å) that are entirely hydrophobic. The polarity of water molecules increases the complexity of interactions. The differential adsorption enthalpy curve shows clear evidence of multistage interactions as a function of water loading: The strongest affinity is at zero coverage, followed by intermediate moderate adsorption and finally by weak gradually decreasing interaction.

An initial sharply rising isotherm associated with strong exothermic heat effects is usually seen when the sorbent features microporosity leading to capillary condensation or strong chemisorption sites binding the adsorbate tightly.[31] It is possible that the microporosity might dictate the competitive binding of water between micropores and unsaturated metal sites in MOFs. Considering the structure and metal site distribution of HKUST-1, either the 4-Å cage or the open Cu site at the 11-Å pore could be responsible for the initial strong water uptake. The 4-Å cage provides tight three-dimensional confinement for an adsorbate molecule, whereas the Cu site in the larger pore offers two-dimensional binding at the pore wall. Theoretical simulations have predicted the magnitude of water adsorption on the unsaturated Cu sites of HKUST-1, suggesting that the binding energy falls into a very narrow range from −47 to −50 kJ/(mol of water),[29,30] in excellent agreement with our observed value of −50.2 kJ/(mol of water). Thus, the series of adsorption events with intermediate strength between approximately 1.5 and 10.5 water molecules per $Cu_3(btc)_2$ molecule (see Figure 3) is very likely to represent the coordination of water molecules onto Cu sites and subsequent pore filling. On the other hand, it is also possible that the most exothermic interaction [0 to roughly 1.5 water molecules per $Cu_3(btc)_2$] might originate from the confinement of water in the smallest micropores (4 Å). Nevertheless, without further experimental evidence, such an assignment appears to be arbitrary. In the present study, two analytical methodologies were developed and coupled to distinguish these intricate interactions.

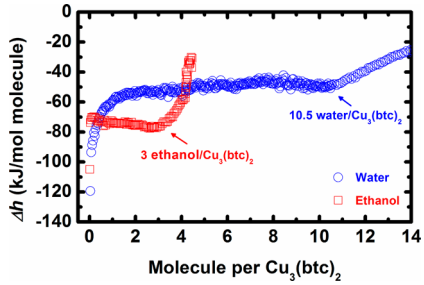


**Figure 3.** Differential enthalpy of adsorption curves for water (navy) and ethanol (red) as a function of the number of moles of molecules adsorbed per mole of $Cu_3(btc)_2$.

To further elucidate the origin of the strong initial interactions, we performed ethanol adsorption calorimetry experiments. We employed ethanol as a probe molecule for two reasons. First, with a kinetic diameter of 4.4 Å, ethanol is just large enough to be excluded by the aperture of the 4-Å cage. Thus, it can interact only with the Cu sites. Furthermore, in the HKUST-1 structure, the ethanol−Cu coordination reaction has a 1:1 stoichiometry, exhibiting no multilayer formation.[16] As a simple polar organic chain, ethanol features a hydroxyl head and a hydrophobic $-CH_2-CH_3$ tail. It can bind with the Cu node, a Lewis acid site, through hydrogen bonding, leaving a much less reactive outward facing $-CH_3$ group. Hupp and co-workers demonstrated that ethanol coordinated to Cu site on HKUST-1 is a poor proton conductor.[16] In other words, the bonded ethanol tends not to form further hydrogen bonds with subsequently introduced free ethanol molecules. A similar phenomenon was observed in our recent study on ethanol−nanocalcite interactions, in which we found that, once an ethanol monolayer is strongly bonded to the nanoparticle surface through its hydroxyl groups, the hydrophobic ends of the adsorbed ethanol interact only very weakly with the second layer of ethanol, resulting in a low-density spatial gap.[24] Figure 3 presents the differential enthalpy of ethanol adsorption on fresh, activated HKUST-1 as a function of the number of molecules adsorbed per $Cu_3(btc)_2$ unit. Interestingly, the tail-like, strongly exothermic heat effects seen in the initial stage of the water adsorption enthalpy profile are missing with ethanol. Instead, the differential enthalpy of ethanol adsorption directly


DOI: 10.1021/acs.jpcc.5b12239
J. Phys. Chem. C 2016, 120, 7562−7567

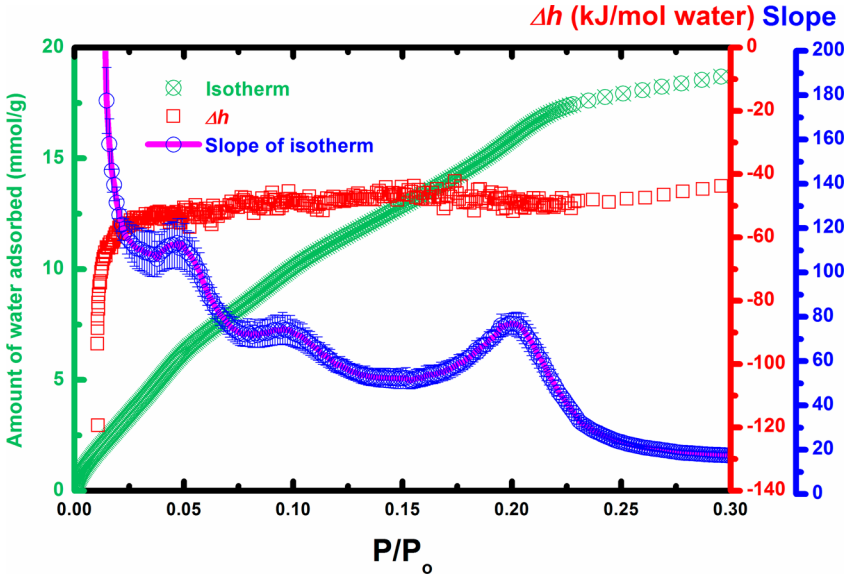


**Figure 4.** Isotherm (green), associated differential enthalpy of adsorption profile (red), and calculated slope curve (blue open circles with pink trace) of the water adsorption isotherm at 25 °C as a function of the partial pressure of water. The width of the curve (standard deviation of the slope at a particular value of $P/P_o$) represents the experimental uncertainty of four reproducible runs.

shows a plateau at roughly −73.6 ± 3.8 kJ/(mol of ethanol). The termination of this plateau at about 3 ethanol molecules per $Cu_3(btc)_2$ strongly suggests that ethanol and the Cu site react with a 1:1 stoichiometry. Such evidence perhaps suggests that the initial strongly exothermic enthalpies of water adsorption prior to the first plateau can be attributed to confinement of water in the 4-Å cage. In the plateau region [from 0 to 3 ethanol molecules per $Cu_3(btc)_2$], the ethanol binding energy profile becomes slightly less exothermic as more ethanol is loaded [centered at −73.6 ± 3.8 kJ/(mol of ethanol)]. This might suggest that the accessibility (effective diameter) of the large pore decreases upon ethanol coordination, leading to increased overall confinement effects. Hence, with combined evidence from water and ethanol adsorption calorimetry, we are able to reveal a potentially sequential filling of water, first into the 4 Å cage, then onto the Cu node, followed by subsequent weak adsorption of water molecules.

Unlike ethanol, coordinated water on Cu makes a good proton donor, which generates a series of water−water clustering events, as described by Hupp and co-workers.[16] The adsorption behavior of water in the 11-Å pore itself is a complex process involving multiple stages, namely, water−Cu coordination, coordinated water−free water binding, and free water condensation. To distinguish these events with similar reaction energetics [centered at −50.2 ± 1.8 kJ/(mol of water)], we took the first derivative (slope) of the water adsorption isotherm. This methodology is inspired by derivative thermogravimetric (DTG) analysis, which is typically applied to interpret weight loss on heating to separate sequential desorption and/or multistage decomposition steps.[32] The strongest adsorption sites usually bind the adsorbate molecules first during adsorption but release them last during desorption. The water adsorption isotherm, differential enthalpies, and calculated slope curve are plotted in Figure 4. The initial slope of the water adsorption curve is nearly infinite but decreases sharply as the partial pressure of water increases. Subsequently, for $0.02 < P/P_o < 0.22$ [between 1.5 and 10.5 water molecules per $Cu_3(btc)_2$], three well-resolved peaks in slope are observed. These peaks are in excellent agreement with the range of the first plateau of the enthalpy profile, suggesting separated water−Cu coordination and subsequent pore filling up to three water molecules per Cu atom (see Figure 4). Subsequently, the slope becomes constant beyond $P/P_o = 0.22$ (see Figure 5 for the full $P/P_o$ range),

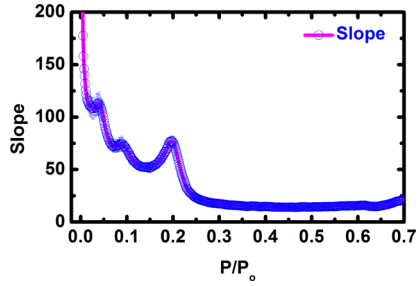


**Figure 5.** Calculated slope curve of the water adsorption isotherm as a function of partial pressure ($P/P_o$) at 25 °C. The width of the error bars on the slope curve (standard deviation of the slope at a particular value of $P/P_o$) represents the experimental uncertainty of four reproducible runs.

corresponding to unfavorable water filling (weak interactions) of the residual space with hydrophobic surfaces. It increases sharply as the remaining pores/cages fill as a result of water condensation. The portion before these three peaks on the slope curve ($P/P_o < 0.02$) corresponds to abrupt water molecule uptake (confinement by the 4-Å cages).

On the other hand, if there is no further binding beyond the direct guest molecule−site coordination, there would merely be one peak in the slope curve. Examples of such behavior include ethanol coordination on HKUST-1 and $CO_2$ adsorption on mmen-$Mg_2$dobpdc[25] [mmen = *N*,*N*′-dimethylethylenediamine, $dobpdc^{4-}$ = 4,4′-dioxido-3,3′-biphenyldicarboxylate; Figure S1]. Therefore, our work also suggests that, although the coordinated and confined water molecules in the 11-Å pores of HKUST-1 are very similar in energetic states, the observed triple-peak slope profile (Figure 5) might indicate the potential



DOI: 10.1021/acs.jpcc.5b12239
J. Phys. Chem. C 2016, 120, 7562−7567

existence of an "onion-like" water configuration with enhanced short-range order, similar to the liquid/solvent restructuring induced by nanoparticle surfaces elucidated by X-ray pair distribution function analysis[33] and calorimetry.[24]

## CONCLUSIONS

In summary, the water−HKUST-1 system has provided a comprehensive model illustrating guest−host interactions in complex hybrid nanoporous materials, in which the enthalpies of interaction/adsorption reflect the interplay and competition between pore structure (three-dimensional confinement from the framework) and surface properties (two-dimensional binding at the metal sites). Specifically, we have measured the enthalpy of water adsorption on HKUST-1, in which heats of adsorption of different strengths were seen, interactions at specific locations were mapped, and potential configurations of water molecules in different pores were suggested. This work demonstrates that the combination of water and ethanol adsorption calorimetry provides a direct and effective pathway to rationally characterize intricate hybrid porous materials containing multiple pore sizes and heterogeneous surfaces. In one such complex system, HKUST-1, three adsorption enthalpies with distinct magnitudes were documented. Moreover, we have developed a new methodology combining the enthalpy of adsorption curve and mathematical analysis of the isotherm to extract adsorption details and enable quantitative separation of a group of binding events having similar enthalpies. Such detailed information can help explain the fundamental principles of interactions at small molecule−MOF interfaces and assist in the design and development of potential applications.

## ASSOCIATED CONTENT

### Supporting Information

The Supporting Information is available free of charge on the ACS Publications website at DOI: 10.1021/acs.jpcc.5b12239.

Calculated slope curve of small molecule−MOF adsorption isotherms (PDF)

## AUTHOR INFORMATION


### Corresponding Author

*E-mail: anavrotsky@ucdavis.edu.


### Notes

The authors declare no competing financial interest.

## ACKNOWLEDGMENTS

This work was supported by the U.S. Department of Energy, Office of Basic Energy Sciences, Grant DE-FG02-05ER15667. The Cornell High Energy Synchrotron Source is supported by National Science Foundation Award DMR-0936384. H.S. thanks the Natural Science Foundation of Shanghai for the financial support (No. 16ZR1408100). The authors thank Manas K. Bhunia and James T. Hughes for providing the MOF material. We also thank Zewei Quan for the synchrotron X-ray scattering analysis and invaluable discussions.

## REFERENCES


(1) Yaghi, O. M.; O'Keeffe, M.; Ockwig, N. W.; Chae, H. K.; Eddaoudi, M.; Kim, J. Reticular Synthesis and the Design of New Materials. *Nature* **2003**, *423*, 705−714.

(2) Kitagawa, H. Metal−Organic Frameworks: Transported into Fuel Cells. *Nat. Chem.* **2009**, *1*, 689−690.

(3) Cook, T. R.; Zheng, Y. R.; Stang, P. J. Metal−Organic Frameworks and Self-Assembled Supramolecular Coordination Complexes: Comparing and Contrasting the Design, Synthesis, and Functionality of Metal−Organic Materials. *Chem. Rev.* **2013**, *113*, 734−777.

(4) Farha, O. K.; Hupp, J. T. Rational Design, Synthesis, Purification, and Activation of Metal−Organic Framework Materials. *Acc. Chem. Res.* **2010**, *43*, 1166−1175.

(5) Furukawa, H.; Cordova, K. E.; O'Keeffe, M.; Yaghi, O. M. The Chemistry and Applications of Metal-Organic Frameworks. *Science* **2013**, *341*, 974−986.

(6) Lee, J.; Farha, O. K.; Roberts, J.; Scheidt, K. A.; Nguyen, S. T.; Hupp, J. T. Metal−Organic Framework Materials as Catalysts. *Chem. Soc. Rev.* **2009**, *38*, 1450−1459.

(7) McDonald, T. M.; Mason, J. A.; Kong, X. Q.; Bloch, E. D.; Gygi, D.; Dani, A.; Crocella, V.; Giordanino, F.; Odoh, S. O.; Drisdell, W. S.; et al. Cooperative Insertion of $CO_2$ in Diamine-Appended Metal-Organic Frameworks. *Nature* **2015**, *519*, 303−308.

(8) Li, J. R.; Kuppler, R. J.; Zhou, H. C. Selective Gas Adsorption and Separation in Metal−Organic Frameworks. *Chem. Soc. Rev.* **2009**, *38*, 1477−1504.

(9) Sumida, K.; Rogow, D. L.; Mason, J. A.; McDonald, T. M.; Bloch, E. D.; Herm, Z. R.; Bae, T. H.; Long, J. R. Carbon Dioxide Capture in Metal−Organic Frameworks. *Chem. Rev.* **2012**, *112*, 724−781.

(10) Venna, S. R.; Carreon, M. A. Highly Permeable Zeolite Imidazolate Framework-8 Membranes for $CO_2/CH_4$ Separation. *J. Am. Chem. Soc.* **2010**, *132*, 76−78.

(11) Bae, Y. S.; Snurr, R. Q. Development and Evaluation of Porous Materials for Carbon Dioxide Separation and Capture. *Angew. Chem., Int. Ed.* **2011**, *50*, 11586−11596.

(12) Peng, Y.; Krungleviciute, V.; Eryazici, I.; Hupp, J. T.; Farha, O. K.; Yildirim, T. Methane Storage in Metal−Organic Frameworks: Current Records, Surprise Findings, and Challenges. *J. Am. Chem. Soc.* **2013**, *135*, 11887−11894.

(13) McKinlay, A. C.; Morris, R. E.; Horcajada, P.; Ferey, G.; Gref, R.; Couvreur, P.; Serre, C. BioMOFs: Metal−Organic Frameworks for Biological and Medical Applications. *Angew. Chem., Int. Ed.* **2010**, *49*, 6260−6266.

(14) Kreno, L. E.; Leong, K.; Farha, O. K.; Allendorf, M.; Van Duyne, R. P.; Hupp, J. T. Metal−Organic Framework Materials as Chemical Sensors. *Chem. Rev.* **2012**, *112*, 1105−1125.

(15) Chui, S. S.-Y.; Lo, S. M.-F.; Charmant, J. P. H.; Orpen, A. G.; Williams, I. D. A Chemically Functionalizable Nanoporous Material. *Science* **1999**, *283*, 1148−1150.

(16) Jeong, N. C.; Samanta, B.; Lee, C. Y.; Farha, O. K.; Hupp, J. T. Coordination-chemistry Control of Proton Conductivity in the Iconic Metal−Organic Framework Material HKUST-1. *J. Am. Chem. Soc.* **2012**, *134*, 51−54.

(17) Borfecchia, E.; Maurelli, S.; Gianolio, D.; Groppo, E.; Chiesa, M.; Bonino, F.; Lamberti, C. Insights into Adsorption of $NH_3$ on HKUST-1 Metal−Organic Framework: A Multitechnique Approach. *J. Phys. Chem. C* **2012**, *116*, 19839−19850.

(18) Kusgens, P.; Rose, M.; Senkovska, I.; Frode, H.; Henschel, A.; Siegle, S.; Kaskel, S. Characterization of Metal-Organic Frameworks by Water Adsorption. *Microporous Mesoporous Mater.* **2009**, *120*, 325−330.

(19) Vishnyakov, A.; Ravikovitch, P. I.; Neimark, A. V.; Bulow, M.; Wang, Q. M. Nanopore Structure and Sorption Properties of Cu-BTC Metal−Organic Framework. *Nano Lett.* **2003**, *3*, 713−718.

(20) Ushakov, S. V.; Navrotsky, A. Direct Measurements of Water Adsorption Enthalpy on Hafnia and Zirconia. *Appl. Phys. Lett.* **2005**, *87*, 164103.

(21) Navrotsky, A.; Mazeina, L.; Majzlan, J. Size-driven Structural and Thermodynamic Complexity in Iron Oxides. *Science* **2008**, *319*, 1635−638.

(22) Navrotsky, A.; Ma, C. C.; Lilova, K.; Birkner, N. Nanophase Transition Metal Oxides Show Large Thermodynamically Driven Shifts in Oxidation-Reduction Equilibria. *Science* **2010**, *330*, 199−201.




DOI: 10.1021/acs.jpcc.5b12239
J. Phys. Chem. C 2016, 120, 7562−7567

(23) Wu, D.; Guo, X. F.; Sun, H.; Navrotsky, A. Energy Landscape of Water and Ethanol on Silica Surfaces. *J. Phys. Chem. C* **2015**, *119*, 15428−15433.
(24) Wu, D.; Navrotsky, A. Probing the Energetics of Organic-Nanoparticle Interactions of Ethanol on Calcite. *Proc. Natl. Acad. Sci. U. S. A.* **2015**, *112*, 5314−5318.
(25) Wu, D.; McDonald, T. M.; Quan, Z.; Ushakov, S. V.; Zhang, P.; Long, J. R.; Navrotsky, A. Thermodynamic Complexity of Carbon Capture in Alkylamine-Functionalized Metal−Organic Frameworks. *J. Mater. Chem. A* **2015**, *3*, 4248−4254.
(26) Wu, D.; Gassensmith, J. J.; Gouvea, D.; Ushakov, S.; Stoddart, J. F.; Navrotsky, A. Direct Calorimetric Measurement of Enthalpy of Adsorption of Carbon Dioxide on CD-MOF-2, a Green Metal−Organic Framework. *J. Am. Chem. Soc.* **2013**, *135*, 6790−9763.
(27) Wu, D.; Guo, X. F.; Sun, H.; Navrotsky, A. Thermodynamics of Methane Adsorption on Copper HKUST-1 at Low Pressure. *J. Phys. Chem. Lett.* **2015**, *6*, 2439−2443.
(28) Bhunia, M. K.; Hughes, J. T.; Fettinger, J. C.; Navrotsky, A. Thermochemistry of Paddle Wheel MOFs: Cu-HKUST-1 and Zn-HKUST-1. *Langmuir* **2013**, *29*, 8140−8145.
(29) Grajciar, L.; Bludsky, O.; Nachtigall, P. Water Adsorption on Coordinatively Unsaturated Sites in CuBTC MOF. *J. Phys. Chem. Lett.* **2010**, *1*, 3354−3359.
(30) Zang, J.; Nair, S.; Sholl, D. S. Prediction of Water Adsorption in Copper-Based Metal−Organic Frameworks Using Force Fields Derived from Dispersion-Corrected DFT Calculations. *J. Phys. Chem. C* **2013**, *117*, 7519−7525.
(31) Furukawa, H.; Gandara, F.; Zhang, Y. B.; Jiang, J. C.; Queen, W. L.; Hudson, M. R.; Yaghi, O. M. Water Adsorption in Porous Metal−Organic Frameworks and Related Materials. *J. Am. Chem. Soc.* **2014**, *136*, 4369−4381.
(32) Sun, H.; Wu, D.; Guo, X. F.; Shen, B. X.; Liu, J. C.; Navrotsky, A. Energetics of Confinement of n-Hexane in Ca-Na Ion Exchanged Zeolite A. *J. Phys. Chem. C* **2014**, *118*, 25590−25596.
(33) Zobel, M.; Neder, R. B.; Kimber, S. A. J. Universal Solvent Restructuring Induced by Colloidal Nanoparticles. *Science* **2015**, *347*, 292−294.



DOI: 10.1021/acs.jpcc.5b12239
*J. Phys. Chem. C* 2016, 120, 7562−7567